

Lieb-Mattis states for robust entangled differential phase sensing

Raphael Kaubruegger,¹ Diego Fallas Padilla,¹ Athreya Shankar,^{2,3} Christoph Hotter,⁴ Sean R. Muleady,^{5,6} Jacob Bringewatt,⁷ Youcef Baamara,¹ Erfan Abbasgholinejad,^{5,6} Alexey V. Gorshkov,^{5,6} Klaus Mølmer,⁴ James K. Thompson,¹ and Ana Maria Rey^{1,8}

¹*JILA, NIST and Department of Physics, University of Colorado, Boulder, Colorado, USA*

²*Department of Physics, Indian Institute of Technology Madras, Chennai 600036, India*

³*Center for Quantum Information, Communication and Computing,
Indian Institute of Technology Madras, Chennai 600036, India*

⁴*Niels Bohr Institute, University of Copenhagen, Blegdamsvej 17, DK-2100 Copenhagen, Denmark*

⁵*Joint Quantum Institute, NIST/University of Maryland, College Park, MD, 20742, USA*

⁶*Joint Center for Quantum Information and Computer Science, NIST/University of Maryland, College Park, MD, 20742, USA*

⁷*Department of Physics, Harvard University, Cambridge, MA 02138 USA*

⁸*Center for Theory of Quantum Matter, University of Colorado, Boulder, Colorado, USA*

Developing sensors with large particle numbers N that can resolve subtle physical effects is a central goal in precision measurement science. Entangled quantum sensors can surpass the standard quantum limit (SQL), where the signal variance scales as $1/N$, and approach the Heisenberg limit (HL) with variance scaling as $1/N^2$. However, entangled states are typically more sensitive to noise, especially common-mode noise such as magnetic field fluctuations, control phase noise, or vibrations in atomic interferometers. We propose a two-node entanglement-enhanced quantum sensor network for differential signal estimation that intrinsically rejects common-mode noise while remaining robust against local, uncorrelated noise. This architecture enables sensitivities approaching the Heisenberg limit. We investigate two state preparation strategies: (i) unitary entanglement generation analogous to bosonic two-mode squeezing, yielding Heisenberg scaling; and (ii) dissipative preparation via collective emission into a shared cavity mode, offering a \sqrt{N} improvement over the SQL. Numerical simulations confirm that both protocols remain effective under realistic conditions, supporting scalable quantum-enhanced sensing in the presence of dominant common-mode noise.

I. INTRODUCTION

Recent advancements in quantum sensors have enabled atomic interferometers [1–3] and optical clocks [4] to reach the fundamental sensitivity limit set by quantum projection noise in ensembles of uncorrelated atoms. Nevertheless, the performance of many state-of-the-art quantum sensors are limited by technical noise sources common to all the atoms, such as the finite coherence time of the electromagnetic fields used for manipulation of the atoms, fluctuations in ambient magnetic fields or vibrations of the optical path of atomic interferometers. A promising strategy to overcome this limitation is the use of quantum sensor networks [5–10]. These networks can be operated in regimes that are insensitive to noise common to all sensor nodes, while preserving sensitivity to spatially varying signals—such as differential frequency shifts between nodes.

Differential phase measurement protocols play a central role in precision metrology, enabling high-accuracy determinations of fundamental constants [1, 11]. They are employed in inertial sensing applications [12, 13] and in experimental tests of the equivalence principle [14–16]. In optical magnetometers operated in a gradiometric configuration, differential sensing can also suppress common-mode magnetic field noise [17–19]. Moreover, networks of optical clocks have recently enabled the observation of gravitational redshift over millimeter-scale height differences [4, 20, 21], as well as differential phase estimation using entangled states [22, 23].

These quantum sensors typically operate with ensembles of N unentangled atoms, which imposes a fundamental limit on their sensitivity. In particular, the variance associated with estimating a phase encoded into the quantum system cannot be reduced below $1/N$, a bound known as the standard quantum limit (SQL) of quantum metrology. Quantum entanglement offers a path to surpass this limitation, enabling measurement precision to approach the Heisenberg limit (HL) of $1/N^2$, the ultimate bound permitted by quantum mechanics [24, 25].

A central challenge in entanglement-enhanced frequency estimation arises from the fact that the attainable uncertainty decreases with increasing interrogation time. At long interrogation times, common-mode noise often emerges as the dominant source of decoherence. While highly entangled states are particularly vulnerable to such noise, unentangled atomic ensembles tend to be more robust. Moreover, the performance of unentangled probes can often be effectively restored through classical post-processing techniques—such as ellipse fitting [26]—which are routinely employed in differential atom interferometry and optical atomic clocks [2, 11, 20, 21, 27–31]. Even though such ellipse fitting strategy can also be extended to a class of entangled states known as spin-squeezed states [32–34], which have recently been realized experimentally [35], in scenarios where sensor performance is constrained by common-phase noise, the degree of useful spin squeezing—and hence the attainable sensitivity enhancement—can be significantly reduced. Consequently, the scaling of sensitivity with N achieved using two spin-

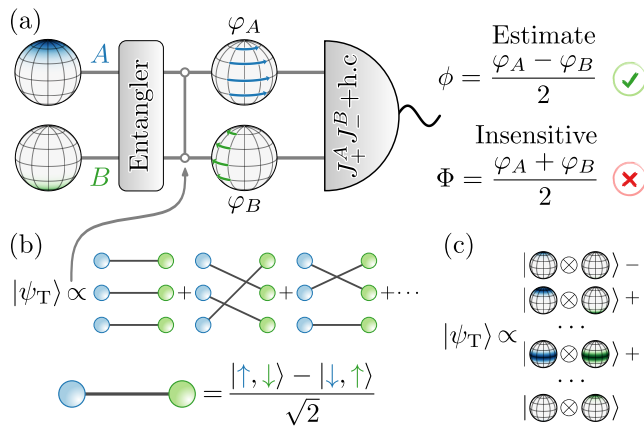


FIG. 1. (a) Schematic illustration of the differential phase sensing protocol. The atoms in ensembles A and B are initially prepared in their respective excited ground states, after which an entangling operation is applied. Subsequently, each ensemble acquires a distinct phase φ_A and φ_B . Finally, a joint measurement of both ensembles is carried out to estimate the differential phase ϕ with high precision, while remaining insensitive to fluctuations of the common phase Φ . (b) The target state after the entangling process, $|\psi_T\rangle$, is an entangled Lieb-Mattis state (see Appendix C) that can be understood as a permutation symmetric superposition over all states where each atom in A forms a singlet with an atom in B . (c) In the Dicke basis of the individual ensembles, represented by their Wigner distributions, this state can be expressed as an equal superposition, with alternating signs, of all Dicke-state combinations where the number of atoms in the excited state in ensemble A equals the number of ground-state atoms in ensemble B .

squeezed ensembles falls short of the ideal scaling expected in the absence of noise [36].

A viable strategy to restore Heisenberg-limited scaling while preserving robustness against laser noise is to operate the sensor network within a decoherence-free subspace [37–41]. This is achieved by preparing entangled states and performing measurements that commute with the noise-generating operators, thereby rendering the system insensitive to common-mode noise by construction. DFS-based techniques have recently been experimentally demonstrated in a system of three trapped ions [42].

The optimal states for differential phase measurements in this setting are typically variants of Greenberger–Horne–Zeilinger (GHZ) states that lie within the DFS. These states can, in principle, achieve HL precision, reducing the estimator variance to $1/N^2$ [43]. However, GHZ states are notoriously fragile: they are extremely sensitive to local noise, which complicates their use in practical systems containing many atoms per sensor node.

In this work, we investigate an alternative family of DFS states that retain Heisenberg scaling but promise significantly improved robustness to local noise than GHZ states. Moreover, GHZ states require sampling an N -body operator, a task that is often prohibitively challenging in many sensing platforms; while local measurements are

sufficient to access an N -body observable, a single local error immediately invalidates the measurement outcome. The states we identify in this manuscript, in contrast require the measurement of two-body operators only to retrieve the encoded phase information. This reduces the technical complexity of implementing a differential sensor network with HL precision. We further propose practical schemes to generate these robust entangled states by harnessing cavity-mediated interactions between sensor nodes.

The remainder of the manuscript is organized as follows. In Sec. II, we introduce the formalism for differential phase sensing with two nodes, each comprising an ensemble of spin-1/2 atoms. Sec. II A reviews the concept of a DFS and explains how it can eliminate the effects of common laser noise, followed by a discussion in Sec. II B of the fundamental limits on sensor precision. In Sec. III, we describe the notion of a robust differential sensor, starting with the optimal two-body observable in Sec. III A, then identifying in Sec. III B a target entangled state that, achieves Heisenberg scaling while being less susceptible to local noise than a GHZ-state. Sec. IV details two practical methods for generating entanglement between sensor nodes via a shared cavity [44]. In Sec. IV A, we propose a unitary preparation scheme based on a bosonic two-mode squeezing interaction realizable with multilevel alkaline-earth atoms, while Sec. IV B discusses a stochastic preparation approach that exploits collective emission. Although this latter method yields only a \sqrt{N} improvement beyond the SQL (rather than full Heisenberg scaling), it can be directly implemented on present-day experiments and is robust to particle-number fluctuations, a significant concern in cavity-based experiments. Finally, Sec. V concludes with a summary and outlook for future applications.

II. DIFFERENTIAL PHASE SENSING

We consider a quantum sensor that consists of N atoms separated into two ensembles A and B with $N_A = N_B = N/2$ atoms per ensemble, with a long-lived transition coupling the states $|\downarrow\rangle$ and $|\uparrow\rangle$. The dynamics of this effective spin-1/2 system are described by the Pauli operators $\sigma_{x,y,z}$, and the whole system can be described by the collective spin operators $J_\alpha^K = \sum_{k=1}^{N_K} \sigma_\alpha^{(k)}/2$ of the respective ensembles, where $\alpha = x, y, z$ and $K = A, B$.

In the interferometric sequence that we will study in this manuscript, the quantum system is first prepared in a potentially entangled quantum state $|\psi\rangle$. Thereafter, the phases φ_A and φ_B are encoded onto the quantum system according to

$$|\psi_{\varphi_A, \varphi_B}\rangle = e^{-i(\varphi_A J_z^A + \varphi_B J_z^B)} |\psi\rangle = U(\varphi_A, \varphi_B) |\psi\rangle. \quad (1)$$

The final step is to perform a measurement $\mathcal{M} = \sum_\mu \mu |\mu\rangle \langle \mu|$ on the quantum system and convert the measurement outcomes μ into an estimate of the encoded phase.

The objective is to optimize the precision in estimating the differential phase $\phi = \frac{\varphi_A - \varphi_B}{2}$, encoded by the operator $J_z^- = J_z^A - J_z^B$, while ensuring that the interferometer remains insensitive to the common phase $\Phi = \frac{\varphi_A + \varphi_B}{2}$, encoded by the operator $J_z^+ = J_z^A + J_z^B$.

The common phase fluctuations can be mitigated by preparing a product state between the two subensembles and then performing repeated measurements of the same differential phase while the common phase varies randomly between measurement repetitions. In each repetition, independent measurements on the two subensembles yield estimates of the phases φ_A and φ_B , which collectively trace out an ellipse whose geometry depends on the differential phase ϕ [26]. This approach has been experimentally demonstrated using ensembles of unentangled atoms [20, 21] as well as spin-squeezed states [35].

However, the practical utility of spin-squeezed states in such measurements is fundamentally limited. In contrast to unentangled ensembles, spin-squeezed ensembles exhibit phase-dependent measurement noise: while the noise can be reduced for certain phase values, it simultaneously increases for others. When the common phase fluctuates randomly across measurement repetitions, the sensor effectively samples the full range of phase-dependent noise. As a result, spin-squeezed states that achieve a reduction of the estimator variance by a factor of $N^{-2/3}$ or more are already too strongly squeezed to operate effectively in such a differential measurement scenario. For moderately squeezed states, the maximum achievable reduction in estimator variance scales as $N^{-1/3}$ [36]. See Appendix A for further discussion.

A. Decoherence free subspace

An alternative approach is to render the sensor inherently insensitive to the common phase by operating the quantum sensor within a DFS with respect to the operator J_z^+ .

Operating in a DFS is achieved by preparing an eigenstate of J_z^+ , ensuring that any random fluctuations in the common phase result only in an irrelevant global phase factor. Additionally, measurements must be performed using an operator that commutes with J_z^+ , thereby making the measurement outcomes independent of the averaging over Φ .

From this point onward, we restrict our analysis to unitary operations and measurements that commute with J_z^+ , and thus do not couple different DFSs. Although we account for noise processes that lead to mixed states with populations distributed across multiple DFSs, these processes do not induce coherences between them. Consequently, the quantum state remains independent of Φ at all times, and we therefore omit the dependence on Φ in all subsequent expressions.

B. Sensor precision

The encoded phase is estimated by performing repeated measurements of the observable \mathcal{M} over r repetitions and using the sample mean of the outcomes to invert the functional dependence of the expectation value $\langle \mathcal{M}_\phi \rangle \equiv \langle \psi | U^\dagger(\phi) \mathcal{M} U(\phi) | \psi \rangle$ on ϕ , where $U(\phi) = e^{-i\phi J_z^-}$. The variance of this estimator is determined via error propagation

$$\Delta_\phi^2 = \frac{\langle \mathcal{M}_\phi^2 \rangle - \langle \mathcal{M}_\phi \rangle^2}{r \left| \frac{\partial}{\partial \phi} \langle \mathcal{M}_\phi \rangle \right|^2}. \quad (2)$$

In the limit of many repeated measurements r , the sensor becomes unbiased, meaning that the average value of the estimator for a given phase converges to the true encoded phase. In this regime, the estimator's performance can be directly compared to fundamental bounds established for unbiased estimators. The variance of an unbiased estimator is lower bounded by the quantum Cramér–Rao bound (QCRB) [24, 25, 45–47],

$$\Delta_\phi^2 \geq \frac{1}{r F_{|\psi\rangle}^{\text{Q}}}, \quad (3)$$

where $F_{|\psi\rangle}^{\text{Q}}$ represents the quantum Fisher information (QFI) of the state $|\psi\rangle$. The QFI quantifies the best precision that can be achieved in parameter estimation for a given quantum state across all physically realizable measurements and estimators. Quantitatively, for a pure state and a unitary parameter encoding, the QFI can be expressed in terms of the variance of the operator responsible for phase encoding:

$$F_{|\psi\rangle}^{\text{Q}} = 4 \left(\langle \psi | J_z^- J_z^- | \psi \rangle - \langle \psi | J_z^- | \psi \rangle^2 \right). \quad (4)$$

The fundamental quantum limit on the estimator variance for a sensor comprising N unentangled atoms is given by $\Delta_\phi^2 \geq 1/N$, known as the standard quantum limit. This bound can be surpassed through the use of entanglement, but cannot be improved beyond the HL, $\Delta_\phi^2 \geq 1/N^2$.

It is straightforward to observe that the state

$$|\psi_{\text{HL}}\rangle = \frac{|\uparrow, \dots, \uparrow\rangle |\downarrow, \dots, \downarrow\rangle + |\downarrow, \dots, \downarrow\rangle |\uparrow, \dots, \uparrow\rangle}{\sqrt{2}}, \quad (5)$$

that corresponds to a GHZ-state and a local π -rotation on ensemble B reaches the HL and hence maximizes the QFI. The state $|\psi_{\text{HL}}\rangle$ is also an eigenstate of J_z^+ and thus resides in a DFS, rendering it insensitive to fluctuations in the common phase. These characteristics make this state particularly appealing for preparation in quantum sensors, as it offers enhanced sensitivity to the desired signal. However, this amplified sensitivity also extends to most noise sources present in current quantum sensing platforms, making the preparation of large-scale GHZ states exceptionally challenging. Consequently, the generation

of GHZ states has become a benchmark for evaluating the capabilities of quantum computing platforms [48–50], with current efforts achieving GHZ-state sizes of up to 32 qubits [51].

Throughout the remainder of this work, we evaluate the performance in terms of the r -independent contribution to the estimator variance, which corresponds to the case $r = 1$.

III. ROBUST DIFFERENTIAL PHASE SENSING

A. Two-body observable

Another fundamental challenge associated with employing GHZ states for quantum-enhanced sensing is the requirement to either reconstruct the full distribution of measurement outcomes through repeated measurements or to estimate an N -body operator, such as $M = \prod_{k=1}^N \sigma_x^{(k)}$ [43]. Measurements of N -body operators are highly susceptible to noise, particularly detection noise, as a single erroneous outcome can invalidate the entire result. In contrast, measurements of single- or two-body operators over an ensemble allow for effective averaging over a limited number of errors. To facilitate the implementation of large-scale entangled sensors, it is therefore advantageous to develop measurement protocols that prioritize single- and two-body observables.

In our DFS, the expectation values of the single-particle observables $\sigma_{x,y}^{(k)}$ vanish. This is because these operators measure coherences between states that differ in the number of excited atoms by 1. Consequently, to obtain a non-trivial measurement outcome, it is necessary to consider an observable composed of at least two-body operators. The only two-body operators that do not commute with the phase encoding and measure coherences within a given DFS—without coupling DFSs with different number of atoms in the excited state—are of the form $\sigma_+^{(k)} \sigma_-^{(l)}$, where $2\sigma_{\pm}^{(k)} = \sigma_x^{(k)} \pm i\sigma_y^{(k)}$, and the indices k and l refer to atoms from different ensembles.

One might be tempted to employ conventional two-body observables that include terms coupling different DFSs, such as $J_x^A J_x^B$, based on the assumption that these couplings do not influence the expectation value of the measurement. However, while the mean signal remains unaffected, such terms lead to an increased measurement variance due to second-order processes involving coupling to other decoherence-free subspaces and back.

The only two-body observable that satisfies the conditions of not containing any terms that commute with the phase encoding, not coupling different DFSs, and being permutationally invariant within the subensembles is

$$\mathcal{M} = J_+^A J_-^B + J_-^A J_+^B, \quad (6)$$

where $J_{\pm}^K = J_x^K \pm iJ_y^K$. Note the distinction between these collective spin raising and lowering operators and the common and differential phase operators J_z^{\pm} . Expressing \mathcal{M}

in the transformed frame yields $\mathcal{M}_{\phi} = U^{\dagger}(\phi)\mathcal{M}U(\phi) = \cos(2\phi) (J_+^A J_-^B + \text{h.c.}) + i \sin(2\phi) (J_+^A J_-^B - \text{h.c.})$. Therefore, the measured expectation value of \mathcal{M} exhibits interference fringes. However, unlike conventional Ramsey fringes, the response to the phase ϕ is doubled, reflecting the fact that a two-body observable is being measured rather than a single-body observable. See Appendix B for a discussion on the implementation of a measurement scheme that mimics the optimal measurement in a cavity-based setup, realized by detecting photons emitted from the cavity while it is tuned into resonance with the atomic transition frequency, following the phase encoding.

For a practical implementation of the quantum sensor, it is desirable to identify initial states that simultaneously exhibit both a large interference fringe contrast and a low measurement variance. However, achieving this balance inherently involves a trade-off: increasing entanglement enhances the QFI and thereby reduces the estimator variance, but at the cost of a reduced fringe amplitude, and vice versa.

In the following section, we present a quantum state characterized by QFI and fringe amplitude that both exhibit optimal scaling as N^2 . Furthermore, we demonstrate that the measurement of \mathcal{M} achieves the QCRB for this initial state.

B. Entangled target state

Since the phase encoding operator J_z^- and the measurement \mathcal{M} are invariant under permutations within each subensemble, a highly sensitive state should exhibit the same symmetry. Consequently, we restrict our analysis to states that are eigenstates of $\mathbf{J}^K \cdot \mathbf{J}^K$ with the maximum eigenvalue $\frac{N}{4}(\frac{N}{4} + 1)$, thereby preserving the subensemble permutation symmetry for $K = A, B$. Here, $\mathbf{J}^K = (J_x^K, J_y^K, J_z^K)^T$ represents the vector of the three collective spin operators for the respective subensemble $K = A, B$ and $\mathbf{J} = \mathbf{J}^A + \mathbf{J}^B$. States respecting this symmetry can be expressed in terms of the basis states $|\frac{N}{4}, M^A, \frac{N}{4}, M^B\rangle$, which satisfy $J_z^K |\frac{N}{4}, M^A, \frac{N}{4}, M^B\rangle = M^K |\frac{N}{4}, M^A, \frac{N}{4}, M^B\rangle$. This basis is related to the $|J, M\rangle$ basis, which are eigenstates of $\mathbf{J} \cdot \mathbf{J}$ and J_z^+ , via the Clebsch-Gordan coefficients $\langle J, M | \frac{N}{4}, M^A, \frac{N}{4}, M^B \rangle$. Note that $|J, M\rangle$ of an ensemble of atoms are generally degenerate for $J < N/2$; however, imposing permutation symmetry within the subensembles ensures that the $|J, M\rangle$ states are unique.

Furthermore, restricting the analysis to states within the DFS in which $N/2$ atoms occupy the excited state constrains the states to the form

$$|\psi_{\text{DFS}}\rangle = \sum_{M=-\frac{N}{4}}^{\frac{N}{4}} c_M |\frac{N}{4}, M, \frac{N}{4}, -M\rangle. \quad (7)$$

When the coefficients c_M are chosen to be $\propto [-\tanh(\alpha)]^{N/4-M}$, these states form a family of states

that mimics bosonic two-mode squeezed states within a spin system [52–54], where α is the squeezing strength. The maximally two-mode squeezed state corresponds to the limit $\alpha \rightarrow \infty$, where the state coincides with the ground state of the Lieb-Mattis Hamiltonian (see Appendix C)

$$|\psi_T\rangle = \frac{1}{\sqrt{\frac{N}{2} + 1}} \sum_M (-1)^{\frac{N}{4} - M} |\frac{N}{4}, M, \frac{N}{4}, -M\rangle. \quad (8)$$

The Lieb-Mattis state, illustrated in Fig. 1(b), is the state symmetrized over all permutations within each subsystem in which each atom in one ensemble forms a singlet with an atom in the other ensemble. Similarly a macroscopic singlet state, in which each atom forms a singlet with every other atom, has previously been proposed as a resource for estimating a field gradient [55]. However, such a state inherently breaks permutation invariance within each subensemble.

The distinctive structure of $|\psi_T\rangle$ as a superposition of pairwise entangled atoms, in contrast to the globally entangled GHZ state, features entanglement that is inherently robust against atom loss [56–59]. The same robustness applies when an atom decays from the excited state to the ground state, effectively projecting itself and its singlet partners into the ground state that cannot acquire a phase and is thus lost for sensing purposes. Recent results further indicate that such robustness to particle loss signifies that the entanglement enhancement is likely to persist under moderate loss of atoms [60], whereas losing even a single particle destroys the useful entanglement in a GHZ state. While spin-squeezed states exhibit similar resilience, the objective of this manuscript is to introduce entangled states and measurement protocols that not only offer robustness but also achieve a scalable improvement in the estimator variance beyond what is possible with two spin-squeezed ensembles.

The state $|\psi_T\rangle$ is uniquely characterized as the eigenstate of $\mathbf{J} \cdot \mathbf{J}$ with eigenvalue zero and of $\mathbf{J}^K \cdot \mathbf{J}^K$ with eigenvalue $\frac{N}{4} (\frac{N}{4} + 1)$. It satisfies both criteria outlined in the preceding section. Accordingly, we refer to this state as the “target state” in the context of the state-preparation protocols considered in this manuscript. Specifically, the measurement expectation value as a function of the encoded phase is

$$\begin{aligned} \langle \psi_T | \mathcal{M}_\phi | \psi_T \rangle &= -\frac{N^2 + 4N}{12} \cos(2\phi), \\ \langle \psi_T | \mathcal{M}_\phi^2 | \psi_T \rangle &= \frac{N^2 + 4N}{240} \left(N^2 + 4N + 8 + \right. \\ &\quad \left. (N^2 + 4N - 12) \cos(4\phi) \right), \end{aligned} \quad (9)$$

and thus the fringe amplitude $(N^2 + 4N)/12$ scales asymptotically as N^2 , which is the maximum scaling achievable for a two-body observable with N^2 terms. Moreover, the estimator variance is minimized at $\phi = \pi/4$, corresponding to the zero crossings of the interference fringes,

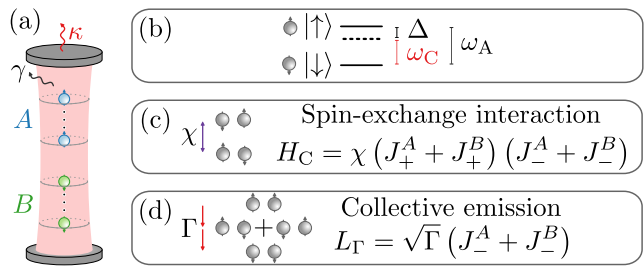


FIG. 2. (a) Schematic of the cavity setup. Two ensembles of atoms, labeled A and B , trapped in a magic-wavelength optical lattice (gray ellipses) inside a cavity and are initially prepared in the excited and ground state, respectively. Photons leak out of the cavity at a rate κ , and atoms in the excited state can emit photons into free space at a rate γ . (b) The cavity mode frequency ω_C is detuned by Δ from the atomic transition frequency ω_A , which quantifies the energy difference between $|\downarrow\rangle$ and $|\uparrow\rangle$. (c) Spin-exchange interactions, described by the Hamiltonian H_C , are mediated by the exchange of virtual photons through the cavity mode. (d) The atoms can collectively emit into the cavity mode. This process is described by the jump operator L_Γ .

achieving the QCRB. The bound is characterized by the QFI

$$F_{|\psi_T\rangle}^Q = \frac{4N + N^2}{3}, \quad (11)$$

which is derived in Appendix F. The QFI, like the fringe amplitude, asymptotically exhibits the best possible scaling, deviating only by a factor of three from the fundamental HL. Having established that the Lieb-Mattis state is a desirable state for robust entanglement enhanced differential sensing we will proceed in the next sections by describing methods for preparing this state and proxies of this state in a cavity system.

IV. STATE PREPARATION

We consider a cavity setup as the one depicted in Fig. 2, where atoms are confined in a deep one-dimensional magic-wavelength optical lattice within an optical cavity, effectively suppressing their motion along the lattice. A single cavity mode, characterized by an angular frequency ω_C and power decay rate κ , couples to a long-lived transition between an excited state $|\uparrow\rangle$ and a ground state $|\downarrow\rangle$ with single-photon Rabi frequency of $2g$. The atomic transition has an angular frequency ω_A and a natural decay rate $\gamma \ll \kappa$.

In the far-detuned limit, $|\Delta| = |\omega_A - \omega_C| \gg \kappa, g\sqrt{N}$, the cavity field can be adiabatically eliminated, while virtual photons mediate effective unitary interactions between the atoms, which can be described by the effective spin Hamiltonian [61]

$$H_C = \chi (J_+^A + J_+^B) (J_-^A + J_-^B). \quad (12)$$

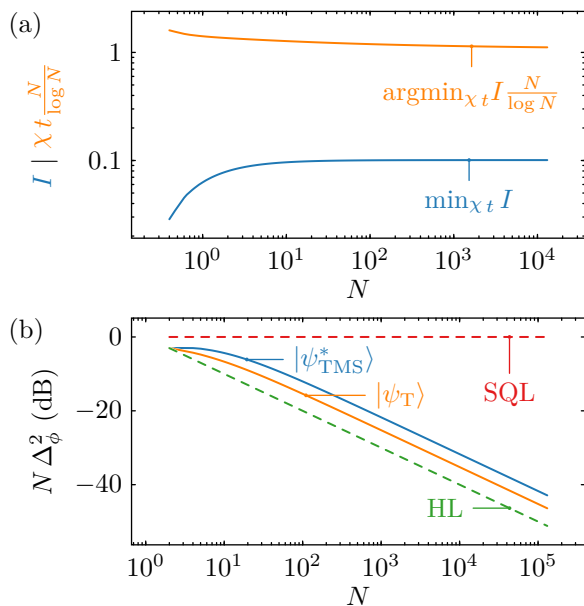


FIG. 3. (a) The minimized infidelity $I = 1 - |\langle \psi_T | \psi_{\text{TMS}}(t) \rangle|^2$, between the target state $|\psi_T\rangle$ and a state that is generated by quenching the product state $|\psi_0\rangle$ under the two-mode squeezing Hamiltonian H_{TMS} [Eq. (13)] (blue). The optimal time required to reach the minimized infidelity for different atom numbers (orange). (b) Scaling of the estimator variance of the quenched state $|\psi_{\text{TMS}}^*\rangle$ at the optimal time and phase $\phi_0 = \pi/4$ in comparison to the target state $|\psi_T\rangle$ and the standard quantum and HL.

The interaction strength $\chi = 4g^2\Delta / (4\Delta^2 + \kappa^2)$ can be tuned by changing the detuning Δ . In order to realize a spin Hamiltonian of this particular form, the atoms need to couple uniformly to a single cavity mode, which can be achieved by trapping the atoms in a lattice with the right spacing or in a ring cavity.

Besides unitary interactions, photons leaking out of the cavity also lead to dissipation in the form of collective emission, described by the collective jump operator $L_\Gamma = \sqrt{\Gamma/2} (J_-^A + J_-^B)$, where $\Gamma = 4g^2\kappa / (4\Delta^2 + \kappa^2)$. By increasing the detuning Δ , the ratio Γ/χ can, in principle, be made arbitrarily small, thus suppressing collective decay. However, this also reduces the overall interaction strength χ , eventually making emission into free space, at rate γ , the dominant source of decoherence. The jump operator describing free-space emission from the excited state of atom k is given by $L_\gamma^{(k)} = \sqrt{\gamma}\sigma_-^{(k)}$, where k indexes the atoms in both ensembles. In practice, one must therefore choose a detuning that balances the detrimental effects of collective and free-space emission to minimize decoherence. The so-called collective cooperativity parameter, $NC = 4Ng^2/(\kappa\gamma)$, determines the effectiveness of state preparation in the presence of these effects.

In Section IV A, we discuss two methods for preparing or approximating the target state by considering only the unitary part of the cavity Hamiltonian. In contrast, in Section IV B, we propose an alternative route to gen-

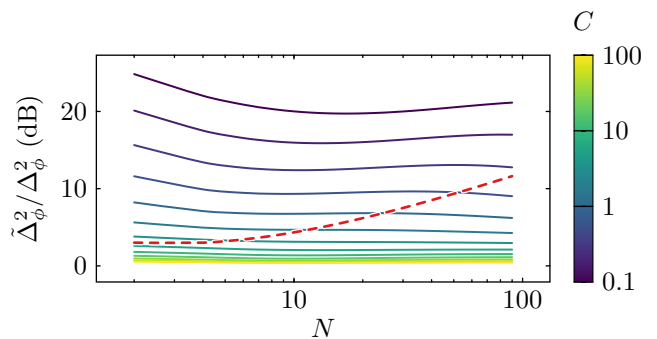


FIG. 4. The optimal estimator variance, denoted as $\tilde{\Delta}_\phi^2$, attainable under a quench with the two-mode squeezing Hamiltonian while simultaneously being subject to collective and free-space emission. It is evaluated relative to the ideal variance achievable in the absence of collective and free-space emission, denoted as Δ_ϕ^2 . $\tilde{\Delta}_\phi^2$ is optimized with respect to the quench duration and the detuning between the cavity and the atomic transition frequency. The red dashed line marks the particle number N at which the standard quantum limit (SQL) is exceeded for a given single-particle cooperativity C .

erate a proxy of the target entangled state by starting from a suitably chosen initial product state and directly employing collective dissipation.

A. Unitary generation of entanglement

An approach to preparing the target state is to initialize the system in the state $|\psi_0\rangle = |N/4, +N/4, N/4, -N/4\rangle$, where all atoms in ensemble A are in the excited state, and all atoms in ensemble B are in the ground state. By adiabatically sweeping a field gradient $H_\delta(t) = -\delta(t) (J_z^A - J_z^B)$ in addition to the cavity Hamiltonian, from $\delta/\chi \gg 1$ to $\delta/\chi \ll 1$, the target state can be prepared with arbitrarily high fidelity, provided the sweep is sufficiently slow (see Appendix D). This is because the target state corresponds to the ground state of the cavity Hamiltonian when permutation symmetry within each subensemble is imposed, whereas the initial state is an eigenstate of the field gradient. However, with decoherence rates competing with the unitary dynamics, achieving a sweep that is adiabatic and at the same time fast enough compared to the decoherence rates requires $C \gg 1$. This condition poses a significant challenge for currently available cavity systems, which typically operate in the regime $C \approx 1$.

A more practical approach in the presence of decoherence is to generate a proxy of the target state by performing a quench using a Hamiltonian of the form

$$H_{\text{TMS}} = \chi i (J_+^A J_-^B - J_-^A J_+^B), \quad (13)$$

applied to the same initial state $|\psi_0\rangle$. This Hamiltonian can be viewed as the atomic analog of the bosonic Hamiltonian responsible for generating two-mode squeezing [53]. Such a Hamiltonian can be implemented by introducing additional one-axis twisting interactions of the form

$H_{\text{OAT}} = \chi (J_z^A J_z^A + J_z^B J_z^B)$ to a spin-exchange Hamiltonian. This addition effectively cancels the interactions within each subensemble, since $\mathbf{J}^K \cdot \mathbf{J}^K = J_+^K J_-^K + J_z^K J_z^K$ does not generate dynamics when the instantaneous state is an eigenstate of this operator. In Appendix E, we detail a potential method for realizing this interaction with multi-level atoms in a cavity. Note that the Hamiltonian derived in Appendix E is equivalent to the expression in Eq. (13) up to a rotation generated by J_z^- . Specifically, $i (J_+^A J_-^B - J_-^A J_+^B) = e^{+i\frac{\pi}{4} J_z^-} (J_+^A J_-^B + J_-^A J_+^B) e^{-i\frac{\pi}{4} J_z^-}$.

Figure 3 (a) illustrates the outcome of a quench designed to minimize the infidelity $I = 1 - |\langle \psi_{\text{TMS}}(t) | \psi_{\text{T}} \rangle|^2$ between the quenched state $|\psi_{\text{TMS}}(t)\rangle = e^{-iH_{\text{TMS}} t} |\psi_0\rangle$ and the target state. Notably, the infidelity asymptotically approaches a finite value of approximately 0.1. It is worth emphasizing that the quench dynamics under purely unitary evolution is constrained to happen in a DFS with $N/2$ atoms in the excited state, whose dimension grows linearly with N . Therefore, an exponential increase in infidelity, as observed in genuine many-body systems, is not expected. Nevertheless, it is remarkable that the infidelity asymptotically approaches a finite value significantly below 1.

An additional encouraging result is that the value of χt that minimizes the infidelity, despite lying beyond the regime of validity of the standard Holstein–Primakoff approximation [53, 54, 62] still exhibits a linear decrease with system size, up to a logarithmic correction. Time scales that decrease as $\log N/N$ are beneficial if the unitary interaction competes with spatially uncorrelated noise such as free-space emission. The optimal sensitivity of the quenched state is shown in Fig. 3 (b), demonstrating that it asymptotically has the same scaling as the target state, differing only by a constant prefactor of approximately 2.2.

In Fig. 4, we analyze the interplay between the unitary generation of entanglement and the detrimental effects of noise in the system. This is achieved by optimizing over the detuning Δ , which governs the ratios Γ/χ and γ/χ , as well as the quench duration.

For system sizes up to $N \leq 90$, the dynamics of two interacting atomic ensembles subject to both collective and free-space emission can be simulated by exact diagonalization of the Lindblad master equation. This is made computationally tractable by restricting the evolution to a Liouville space whose dimension scales as $\propto N^6$, leveraging the permutation symmetry of the free-space decay jump operators [63–66]. For larger particle numbers, a viable approach is to employ a Monte Carlo wavefunction simulation [67].

By optimizing the detuning Δ , a trade-off is achieved that balances the detrimental effects of both collective and free-space emission. Our results indicate that, once the cooperativity-enhanced collective coupling NC is sufficiently large to surpass the standard quantum limit (SQL), the presence of noise does not alter the scaling behavior of the estimator variance compared to the noiseless Heisenberg scaling. Notably, the deviations manifest solely in

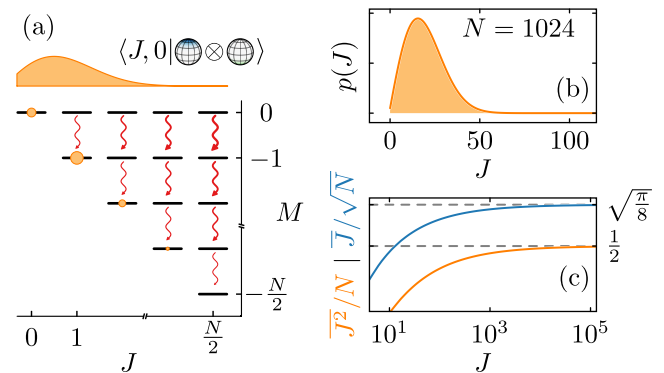


FIG. 5. (a) Collective emission (red curly arrows) evolves the initial state into a steady state, corresponding to a mixture of Dicke states located on the lower diagonal of the Dicke state ladder, characterized by quantum numbers J and M . The steady-state distribution (orange circles) corresponds to the probability of projecting the initial state onto a specific $|J, 0\rangle$ state (orange distribution). (b) The probability of projecting onto a given $|J, 0\rangle$ state, is determined for the initial state where the atoms in ensemble A are in the excited state and those in ensemble B are in the ground state. (c) The first moment, $\bar{J} = \sum_J J p(J)$, and the second moment, $\bar{J}^2 = \sum_J J^2 p(J)$, of the distribution presented in panel (b) are shown for different atom numbers N , rescaled to highlight their respective asymptotic scaling. The dashed lines indicate the prefactors corresponding to the asymptotic scaling.

the prefactor, which increases as C decreases, while the asymptotic scaling remains seemingly unaffected.

Extrapolating this trend to larger values of NC , we anticipate that an enhancement consistent with Heisenberg scaling should be achievable in current cavity-based experiments. Furthermore, the performance of this scheme could be enhanced by dynamically varying the detuning during the quench given that as the instantaneous state approaches the target state during the evolution, the detrimental effect of collective emission diminishes. Consequently, the detuning can be gradually reduced, thereby also decreasing the ratio γ/χ .

In the next section, we introduce an alternative approach that circumvents the need to engineer the desired unitary interactions directly. Instead, we exploit collective superradiance decay as the mechanism for generating metrologically useful entanglement.

B. Stochastic preparation of entanglement

Collective emission becomes the dominant dynamical process when the cavity is tuned close to resonance with the atomic transition frequency. This strong dissipative mechanism can be exploited to generate entanglement. Conceptually, this is akin to the approach in Ref. [68], although that work instead focused on three-level atoms and identified states sensitive to a signal encoded by an operator resembling the two-mode squeezing Hamiltonian

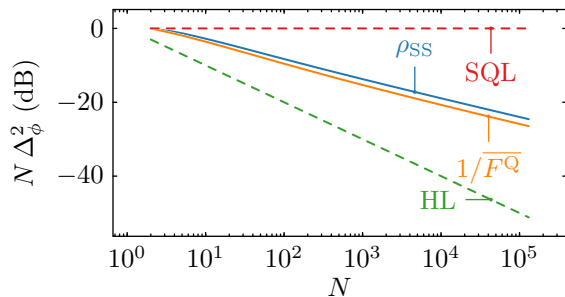


FIG. 6. The estimator variance of the steady state ρ_{SS} [Eq. (15)], prepared via collective emission, is evaluated at the optimal phase $\phi = \pi/4$ for various atom numbers N and the measurement \mathcal{M} . The resulting performance is benchmarked against the QCRB associated with the inverse of the average QFI [Eq. (17)] of the pure states appearing in the spectral decomposition of ρ_{SS} , as well as against the SQL and the HL.

of Eq. (13).

Collective emission will generate an entangled density matrix if it acts on the right initial state. Here we will consider the same initial state $|\psi_0\rangle = |\frac{N}{4}, +\frac{N}{4}, \frac{N}{4}, -\frac{N}{4}\rangle$ as previously. Projecting this state onto the $|J, 0\rangle$ states, which satisfy $\mathbf{J} \cdot \mathbf{J} |J, M\rangle = J(J+1) |J, M\rangle$ and $J_z^+ |J, M\rangle = M |J, M\rangle$, results in the probability distribution shown in Fig. 5(b,c),

$$p(J) = \left| \langle J, 0 | \frac{N}{4}, +\frac{N}{4}, \frac{N}{4}, -\frac{N}{4} \rangle \right|^2 \approx \frac{2J+1}{N/2+1} \left(\frac{N+2-J}{N+2+J} \right)^{J+1}, \quad (14)$$

where the approximation is valid in the limit of asymptotically large N . Figures 5(b,c) further illustrate that, for large N , the distribution becomes asymptotically centered at a value scaling $\propto \sqrt{N}$, with a standard deviation that also scales $\propto \sqrt{N}$. This means that the distribution has a small but finite probability to be in the target state but generally skewed towards small but non-zero values of J .

This probability distribution contains all the necessary information to describe the steady state under collective emission sketched in Fig. 5(a). This follows from the fact that the jump operator $L_\Gamma = \sqrt{\Gamma} J_-$ commutes with $\mathbf{J} \cdot \mathbf{J}$, which ensures that the J quantum number distribution remains invariant under the evolution and merely reduces M , since $J_- |J, M\rangle \propto |J, M-1\rangle$. Consequently, each $|J, M\rangle$ state decays into the corresponding state with the minimal number of excited state atoms, $|J, -J\rangle$. The resulting steady state is therefore given by

$$\rho_{SS} = \sum_{J=0}^{N/2} p(J) |J, -J\rangle \langle J, -J|. \quad (15)$$

The steady state corresponds to a mixture of $|J, -J\rangle$ states, which all possess a large QFI for differential phase sensing:

$$F_{|J, -J\rangle}^Q = \frac{4N + N^2 - 8J - 4J^2}{3 + 2J} \quad (16)$$

at $\phi = \pi/4$ if $J \ll N$, see Appendix F. Furthermore, the states $|J, -J\rangle$ correspond to the Lieb-Mattis ground state when the Lieb-Mattis Hamiltonian is projected onto a DFS with $N/2 - J$ atoms in the excited state.

Figure 6 shows that, in the vicinity of the optimal phase $\phi = \pi/4$, the estimator variance for the steady state exhibits a scaling behavior closely matching the QCRB for the corresponding mixed state (see Appendix G),

$$\frac{1}{\Delta_\phi^2} \leq \overline{F^Q} = \sum_J p(J) F_{|J, -J\rangle}^Q. \quad (17)$$

Numerical calculations reveal asymptotic scaling exponents of -0.50 for the variance and -0.51 for the bound, both corresponding to the same scaling as the state $|\bar{J}, -\bar{J}\rangle$ where \bar{J} is the J that is closest to the mean value $\sum_J J p(J)$.

We draw attention to another opportunity that becomes particularly relevant when the time required to prepare the initial state is short compared to the phase accumulation time. In this regime, measuring the photons leaking out of the cavity is advantageous, because these photons reveal which state $|J, -J\rangle$ has been prepared. With this information, one can restart the state preparation process if the detected photon count is too high (i.e., the J quantum number of the stochastically prepared state is too large). While this procedure can reduce the estimator variance, its effectiveness strongly depends on the relative timescales of the state preparation and the phase accumulation, as well as on the photon count threshold chosen to discard a prepared state.

In Fig. 7, we analyze the influence of free-space emission on the stochastic state preparation process. In the near-resonant bad cavity regime $N\Gamma \approx NC\gamma$, an increase in collective cooperativity enhances the favorable collective emission relative to the detrimental free-space emission rate. Notably, the scaling of the estimator variance remains largely unaffected even as cooperativity decreases.

If this trend persists for larger systems, it suggests that significant improvements beyond the standard quantum limit could be realized for ensembles of a few hundred atoms. Such improvements appear feasible for cooperativity values around $C \approx 0.4$, which are within reach of current experimental setups [61, 69].

Another notable advantage of the stochastic state preparation process is its robustness to fluctuations in the number of atoms within the subensembles. Assuming a fixed total number of atoms with an imbalance of $N^I = |N^A - N^B|$, the probability distribution satisfies $p(J') = 0$ for $J' < N^I$, while the proportions of the distribution remain similar for $J' > N^I$. This can be understood as a consequence of the reduced number of atoms available in one of the ensembles to form singlet pairs. As a result, the unpaired atoms relax to the ground state, leading to a reduction in the total number of excited atoms in the steady state.

Consequently, as long as the imbalance satisfies $N^I \ll \sqrt{N}$, no significant increase in the estimator variance is expected. Additionally, this scheme benefits from the

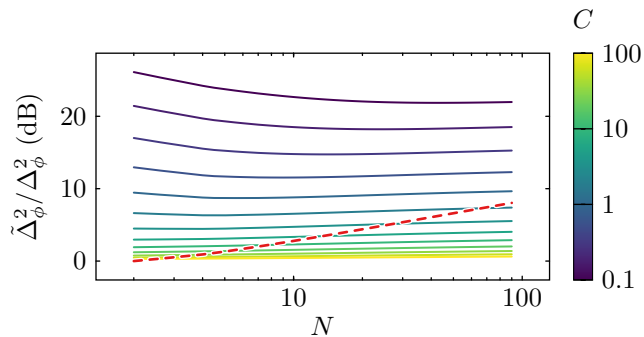


FIG. 7. The optimal estimator variance attainable under stochastic entanglement generation, while being subject to free-space emission, denoted as $\tilde{\Delta}_\phi^2$, is evaluated relative to the variance achievable in the absence of free-space emission, denoted as Δ_ϕ^2 . $\tilde{\Delta}_\phi^2$ is optimized with respect to the duration for which the initial state $|\psi_0\rangle$ undergoes collective and free-space emission. The red dashed line marks the particle number N at which the standard quantum limit (SQL) is exceeded for a given single-particle cooperativity C .

fact that the time required to reach the steady state is not a fine-tuned parameter dependent on specific particle numbers.

V. OUTLOOK

In this work, we have investigated entanglement-enhanced sensing of a phase difference encoded in two atomic ensembles. By leveraging the concept of a DFS, we have analyzed an interferometric scheme that is intrinsically robust against common-mode phase fluctuations. Furthermore, we have identified a specific quantum state which, when combined with an appropriate measurement strategy, yields an estimator variance that scales at the Heisenberg limit, while being robust to commonly encountered noise sources. This state is a superposition of all possible permutations of states in which each atom in ensemble A forms a singlet pair with an atom in ensemble B . A key advantage of this state is its resilience to local errors: a single local error merely projects one of the singlet pairs into a trivial state, whereas, in the case of a maximally entangled GHZ-state, a single local error would collapse the entire many-body state into a trivial, unentangled state.

Having established this state as the optimal target for robust entanglement-enhanced sensing, we have proposed and analyzed two state preparation protocols that exploit cavity-mediated entanglement to approximate the target state. The first protocol relies on an interaction that can be interpreted as a bosonic two-mode squeezing interaction, which for example can be realized using multilevel alkaline-earth atoms, as described in Appendix E.

The second protocol stochastically generates an entangled density matrix via collective emission into the cavity mode. While this approach does not achieve an

estimator variance scaling at the HL, it still offers an improvement over the SQL by a factor scaling as $1/\sqrt{N}$. Which surpasses the scaling achievable with two independently spin-squeezed ensembles in the presence of dominant common-mode noise. Notably, this method is directly implementable in current cavity-based experimental setups and is expected to exhibit robustness against fluctuations in the atom number difference between the two ensembles at the level of \sqrt{N} .

Additionally, we have evaluated the impact of collective and free-space emission on both preparation schemes. Our analysis indicates that while these decoherence mechanisms increase the prefactor of the estimator variance, they do not affect its fundamental scaling. For collective cooperativity values achievable in state-of-the-art experiments, a substantial enhancement beyond the SQL remains feasible.

While our discussion has focused on a cavity-based setup, where entanglement can be generated instantaneously between any pair of particles, a natural extension of this work is the consideration of systems with finite-range interactions. Such interactions naturally arise in a variety of quantum sensing platforms, including optical lattice [70] or tweezer clocks [35], trapped ions [71], and Rydberg atoms [72, 73]. In Appendix C, we discuss a finite-range Hamiltonian that serves as a parent Hamiltonian for the target state, raising the question of whether such a Hamiltonian can be experimentally realized and whether its ground state can be prepared, for instance by an adiabatic ramp or a quench. Other directions to explore are variational methods using parameterized quantum circuits to prepare the ground state, thereby minimizing the achievable estimator variance [74–76] or methods that use mid-circuit measurements and feedback [77].

Extending differential phase to frequency estimation, is relevant for many practical applications. The precision of such frequency estimates improves with an extended interrogation time, during which the atoms interact with the frequency signal. A fundamental limitation to arbitrarily increasing this interrogation time is the finite lifetime of the excited state. To circumvent this constraint, one could employ pairs of fermionic atoms prepared in a dark state, where emission into free space is strongly suppressed [78]. By replacing each sensor atom with such a dark-state pair, this approach effectively removes the fundamental limit on interrogation time, thereby enabling unprecedented sensitivity in differential frequency estimation.

Another promising avenue for future extensions involves applying continuous measurement protocols [79–82], in which for example the photons leaking from the cavity are monitored in real time while the differential phase is simultaneously encoded onto the atomic system. This approach could offer additional pathways to surpass classical sensing limits by continuously tracking the phase evolution.

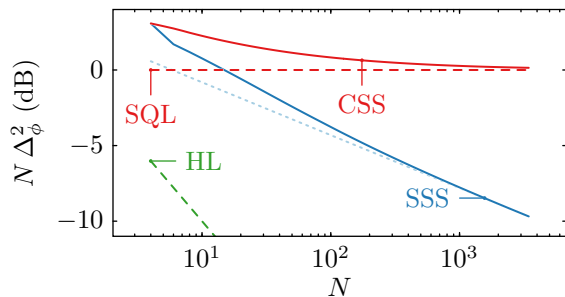


FIG. 8. The Fisher information in Eq. (A2) is evaluated at the phase ϕ that maximizes the Fisher information for a sensor network comprising two coherent spin states (CSS) and two spin-squeezed states (SSS). In the case of spin-squeezed states, the Fisher information is further optimized over the degree of spin squeezing. The dotted lines represent the asymptotic scaling of the Fisher information in the limit of large atom numbers N . The dashed green line corresponds to the fundamental Heisenberg limit, given by $F \leq N^2$.

VI. ACKNOWLEDGMENTS

We thank Marcus Bints for insightful discussions and Maya Miklos, Theodor Lukin Yelin, and Adam Kaufman for useful feedback on the manuscript. This work is supported by the Vannevar Bush Faculty Fellowship, AFOSR FA9550-24-1-0179, the NSF JILA-PFC PHY-2317149 and NSF QLCI awards OMA-2016244 and OMA-2120757, the U.S. Department of Energy, Office of Science, National Quantum Information Science Research Centers, Quantum Systems Accelerator the Heising-Simons foundation and NIST. KM acknowledges the JILA visiting fellows program and support from the Danish National Research Foundation (Center of Excellence “Hy-Q,” grant number DNR139). CH is supported by the Carlsberg Foundation through the “Semper Ardens” Research Project QCool. E.A. and A.V.G. were supported in part by the AFOSR MURI, ARL (W911NF-24-2-0107), DARPA SAVaNT ADVENT, the DoE ASCR Quantum Testbed Pathfinder program (awards No. DE-SC0019040 and No. DE-SC0024220), NSF STAQ program, and NQVL:QSTD:Pilot:FTL and from the U.S. Department of Energy, Office of Science, Accelerated Research in Quantum Computing, Fundamental Algorithmic Research toward Quantum Utility (FAR-Qu).

Appendix A: Separable strategies

In this section, we establish the limits on sensing the differential phase using two spin ensembles, with no entanglement shared between them but allowing for spin squeezing within each ensemble. To achieve this, we employ the classical Fisher information, which provides a lower bound on the sensitivity of any unbiased estimator. This bound, in turn, applies to specific estimation strategies, such as ellipse fitting [2, 11, 20, 21, 26–31].

We examine two scenarios. In the first scenario, both ensembles are initialized in a coherent spin state, denoted as $|\psi_{\text{CSS}}\rangle = e^{-i\frac{\pi}{2}J_y} |\frac{N}{4}, -\frac{N}{4}, \frac{N}{4}, -\frac{N}{4}\rangle$, where all spins are aligned along the x -axis. In the second scenario, the ensembles are prepared in spin-squeezed states using the one-axis-twisting interaction [33], represented as $|\psi_{\text{SSS}}\rangle = e^{-i\nu J_x} e^{-i\mu(J_z^A J_z^A + J_z^B J_z^B)} |\psi_{\text{CSS}}\rangle$, where the parameter ν is chosen such that the direction of the squeezed variance is along the y -axis.

Next, the phase ϕ is encoded onto the respective states according to $|\psi_\phi\rangle = e^{-i\phi J_z^-} |\psi\rangle$. Since both states are not confined to a DFS, it is necessary to account explicitly for random fluctuations of the common phase. This is achieved by considering a density matrix of the form

$$\rho_\phi = \frac{1}{2\pi} \int_0^{2\pi} d\Phi e^{-i\Phi J_z^+} |\psi_\phi\rangle \langle\psi_\phi| e^{+i\Phi J_z^+}. \quad (\text{A1})$$

Here, J_z^- and J_z^+ are the operators associated with the differential and common phases, respectively. Since these operators commute, their effects can be treated consecutively.

The final step of the interferometric sequence involves applying a $\pi/2$ -pulse around the x -axis and independently measuring the population imbalance, M^A and M^B , of each ensemble independently. The conditional probability of observing a specific population imbalance, given the encoded differential phase ϕ , is expressed as

$$p(M^A, M^B|\phi) = \text{tr} \left[\Pi_{M^A, M^B} e^{-i\frac{\pi}{2}J_x} \rho_\phi e^{+i\frac{\pi}{2}J_x} \right], \quad (\text{A2})$$

where $\Pi_{M^A, M^B} = |\frac{N}{4}, M^A, \frac{N}{4}, M^B\rangle \langle\frac{N}{4}, M^A, \frac{N}{4}, M^B|$ is the projection operator onto the state characterized by the specified population imbalances.

The classical Fisher information, derived from the conditional probability distribution, is given by

$$F = \sum_{M^A, M^B} \frac{\left(\frac{\partial}{\partial \phi} p(M^A, M^B|\phi) \right)^2}{p(M^A, M^B|\phi)} \quad (\text{A3})$$

and serves as a lower bound for the estimator variance in Eq. (2), as established by the Cramér-Rao bound (CRB), $\Delta_\phi^2 \geq 1/F$, which is a tighter version of the QCRB that explicitly depends on the measurement. It is important to emphasize that the CRB derived here represents a fundamental lower bound for any unbiased ellipse-fitting method. However, achieving this bound with a maximum likelihood estimator would require precise knowledge of the probability distribution $p(M^A, M^B|\phi)$, which may be challenging to obtain experimentally. Nonetheless, the Fisher information provides a meaningful benchmark for evaluating the performance of the measurement protocols discussed in the main text.

In Fig. 8, the inverse Fisher information for two coherent spin states initially exceeds the standard quantum limit but asymptotically approaches the SQL as N becomes

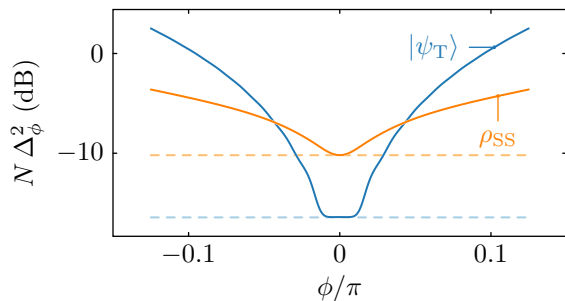


FIG. 9. Estimator variance associated with measuring the number of photons emitted from the cavity after the phase has been encoded, evaluated for both the target state $|\psi_T\rangle$ and the steady state resulting from collective emission ρ_{SS} of a system of $N = 128$ atoms. The dashed lines indicate the corresponding QCRBs.

large. Whereas, independently squeezing the individual ensembles enables surpassing the standard quantum limit; however, the presence of common phase fluctuations diminishes the potential benefits of spin squeezing. In the absence of common phase noise, spin squeezing generated via the one-axis twisting Hamiltonian provides an improvement over the standard quantum limit, with an asymptotic scaling of $N^{-2/3}$ [33]. To determine the asymptotic scaling behavior in the presence of phase noise, we fit the inverse Fisher information optimized over the squeezing strength. The resulting scaling exponent, represented by the dashed blue line in Fig. 8, is found to be -0.35 , which is in agreement with the previously reported exponent of $-1/3$ obtained from ellipse fitting [36]. This notably smaller scaling exponent arises from the fact that the measurement variance of a spin-squeezed state is reduced only for specific phase values, while it increases for others. The presence of random common phase fluctuations leads to a situation where measurement variance is averaged over all phase values. In order to compensate, the optimal amount of squeezing is smaller than in the noiseless case.

This underscores the advantages of a sensor operating within a DFS, where scaling as favorable as N^{-1} can be achieved. Even in the most experimentally realistic scenario, where entanglement is generated via collective emission, the achieved scaling of $N^{-1/2}$ significantly outperforms the scaling of two independently squeezed ensembles.

Appendix B: Measurement

Since the implementation of the optimal measurement specified in Eq. 6 is not straightforward, we propose an alternative measurement scheme capable of saturating the CRB. Specifically, we consider a scenario in which the cavity is suddenly tuned into resonance with the atomic transition frequency (i.e., quenched) after the phase has been encoded in the quantum system. In this regime,

the dynamics are dominated by collective emission described by the jump operator L_Γ . Each quantum jump corresponds to the emission of a photon from the cavity. Assuming that all photons leaking from the cavity are detected until the atomic system reaches a steady state with respect to L_Γ , this measurement effectively corresponds to observing the diagonal spin operator

$$O = (J + M) |J, M\rangle \langle J, M|, \quad (\text{B1})$$

which is diagonal in the $|J, M\rangle$ basis. This interpretation arises from the fact that a state $|J, M\rangle$ decays to $|J, -J\rangle$ via the emission of $J + M$ photons, which, in the bad cavity limit, are rapidly lost and can thus be detected as they exit the cavity.

The estimator variance corresponding to the measurement of the number of photons leaking from the cavity is shown in Fig. 9. For both the target state and the steady state resulting from collective emission, the QCRB is saturated at $\phi = 0$. A limitation of this measurement scheme, however, is that at $\phi = 0$, the target state is an eigenstate of the measurement operator and the steady state is a mixture of eigenstates. Therefore in this limit, both the numerator and denominator of the estimator variance vanish, making the sensor particularly vulnerable to additional noise in the system which overwrites the vanishing numerator and results in a large estimator variance.

Remarkably, the target state exhibits a finite interval of phase values around $\phi = 0$ where the QCRB is still saturated, indicating that the sensor can be operated away from $\phi = 0$ while retaining optimal sensitivity. In contrast, the steady state also achieves the QCRB at $\phi = 0$, but lacks such a robust phase interval. Therefore, in practical implementations, one must trade off some sensitivity in favor of operating at a reference phase where the measurement is less susceptible to residual noise.

In conclusion, while photon counting via cavity leakage allows the QCRB to be saturated, the limited robustness of this measurement to external noise motivates the implementation of the true optimal measurement scheme for enhanced performance.

Appendix C: Lieb-Mattis Hamiltonian

In this section, we discuss the parent Hamiltonian of the target state Eq. (8) which is commonly referred to as the Lieb-Mattis Hamiltonian [83]

$$H_{LM} = 2\chi \mathbf{J}^A \cdot \mathbf{J}^B \\ = \chi (\mathbf{J} \cdot \mathbf{J} - \mathbf{J}^A \cdot \mathbf{J}^A - \mathbf{J}^B \cdot \mathbf{J}^B), \quad (\text{C1})$$

The Lieb-Mattis Hamiltonian serves as a compelling and exactly solvable toy model for investigating ferromagnetism on a square lattice and exploring the mechanism of spontaneous symmetry breaking. As shown in the second line of Eq. (C1), its ground state is characterized by maximizing the expectation values $\mathbf{J}^K \cdot \mathbf{J}^K$ within each

ensemble while minimizing the expectation value of $\mathbf{J} \cdot \mathbf{J}$, ultimately yielding a unique state. This ground state can also be interpreted as a superposition of a continuum of Néel states, each pointing with equal probability in all possible directions on the Bloch sphere [84]. In the thermodynamic limit, this symmetry is spontaneously broken [83]. However, in finite systems, the symmetry can be explicitly broken by a perturbation, such as the phase-encoding Hamiltonian J_z^- , which selects a single Néel state from the continuum of Néel states pointing in different directions.

If the system is restricted to a different DFS, or equivalently to an eigenspace of J_z^+ with eigenvalue $M \neq 0$, the Lieb-Mattis ground state within this subspace corresponds to the simultaneous eigenstate of $\mathbf{J} \cdot \mathbf{J}$ and J_z^+ , $||M\rangle, M\rangle$. These states are uniquely defined under the condition that the expectation value of $\mathbf{J}^K \cdot \mathbf{J}^K$ is maximized. Notably, the estimator variance Eq. (2) for any of these states, in conjunction with a measurement of the optimal two-body observable Eq. (6), achieves the QCRB for $\phi = \pi/4$. The QFI for these states is given by

$$F_{||M\rangle, M\rangle}^Q = \frac{4N + N^2 - 8M - 4M^2}{3 + 2M}, \quad (\text{C2})$$

which exhibits Heisenberg scaling when $M \ll N$. A derivation of this expression for the QFI can be found in Appendix F.

To find a parent Hamiltonian for the target state, it is not strictly necessary to have infinite-range interactions. Instead, it suffices to consider a bipartite lattice model in any dimension, in which nearest-neighbor sites belong to different sublattices, while next-nearest neighbors belong to the same sublattice. The J_1 - J_2 Hamiltonian

$$H_{J_1-J_2} = J_1 \sum_{\langle i,j \rangle} \boldsymbol{\sigma}^{(i)} \cdot \boldsymbol{\sigma}^{(j)} - J_2 \sum_{\langle\langle i,j \rangle\rangle} \boldsymbol{\sigma}^{(i)} \cdot \boldsymbol{\sigma}^{(j)} \quad (\text{C3})$$

is a parent Hamiltonian of the target state, provided that the ratio of nearest-neighbor to next-nearest-neighbor interaction strengths satisfies $J_1/J_2 \ll 1$. Here the summation indices $\langle i,j \rangle$ and $\langle\langle i,j \rangle\rangle$ denote sums over all nearest-neighbor and next-nearest-neighbor pairs, respectively.

Each term in the J_1 - J_2 Hamiltonian commutes with $\mathbf{J} \cdot \mathbf{J}$, ensuring that the ground state is an eigenstate of $\mathbf{J} \cdot \mathbf{J}$. However, the nearest-neighbor interactions do not commute with $\mathbf{J}^A \cdot \mathbf{J}^A$ or $\mathbf{J}^B \cdot \mathbf{J}^B$, implying that the fully permutation-symmetric state within each subensemble is not the ground state unless $J_1/J_2 \ll 1$. In that regime, the J_1 - J_2 Hamiltonian approximately commutes with $\mathbf{J}^A \cdot \mathbf{J}^A$ and $\mathbf{J}^B \cdot \mathbf{J}^B$, causing the ground state to converge to the target state.

Appendix D: Adiabatic preparation

In this section, we provide additional intuition for the adiabatic sweep, which is implemented using the cavity

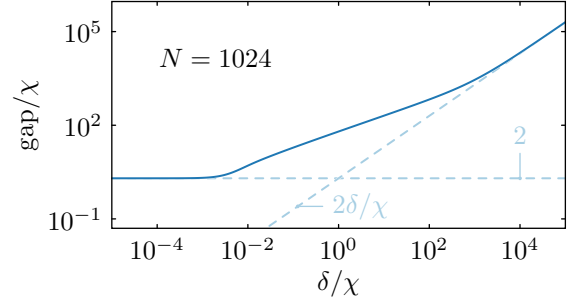


FIG. 10. Energy gap between the ground and first excited state of the Hamiltonian $H = \chi (J_+^A + J_+^B) (J_-^A + J_-^B) + \delta (J_z^A - J_z^B)$ for $N = 1024$ atoms.

Hamiltonian from Eq. (12) in combination with a time-dependent field gradient that is ramped off during as a function of the ramp time t . The resulting Hamiltonian is

$$H_{\text{ad}}(t) = \chi \left(J_+^A + J_+^B \right) \left(J_-^A + J_-^B \right) - \delta(t) \left(J_z^A - J_z^B \right). \quad (\text{D1})$$

and enables the adiabatic preparation of the target state. This state corresponds to the unique ground state of the Lieb-Mattis Hamiltonian introduced in Eq. (C1) $H_{\text{LM}} = J_+ J_- + J_z^2 - \mathbf{J}^A \cdot \mathbf{J}^A - \mathbf{J}^B \cdot \mathbf{J}^B$. The terms $J_z^2, \mathbf{J}^A \cdot \mathbf{J}^A, \mathbf{J}^B \cdot \mathbf{J}^B$, which are required to transform the cavity Hamiltonian into the parent Hamiltonian, commute with all components of the cavity Hamiltonian. Moreover, both the initial state and the final state are eigenstates of these operators with identical eigenvalues. Consequently, these terms do not need to be explicitly included during the adiabatic sweep to achieve the desired target state.

The speed at which the adiabatic sweep can be performed depends on the instantaneous energy gap of the Hamiltonian to the state closest in energy that shares the same symmetries as the cavity Hamiltonian and the initial state. In the two limits $\delta/\chi \gg 1$ and $\delta/\chi \ll 1$, the gap between the ground and first excited state is independent of N and scales with 2δ and 2χ respectively, see Fig. 10. To ensure the success of the sweep, its speed must be small compared to these energy scales while remaining sufficiently fast to avoid perturbations such as free-space or collective emissions that could take the system out of the symmetry subspace. However, achieving this balance poses challenges under typical cavity parameters that rely on the collective cooperativity NC and not just C .

Appendix E: Realizing a two-mode squeezing interaction with multi-level alkaline earth atoms

In this section, we present a potential implementation of the two-mode squeezing interaction described by Eq. (13). Our focus is on alkaline-earth atoms with large nuclear spin, such as ^{87}Sr . We select the nuclear spin quantization

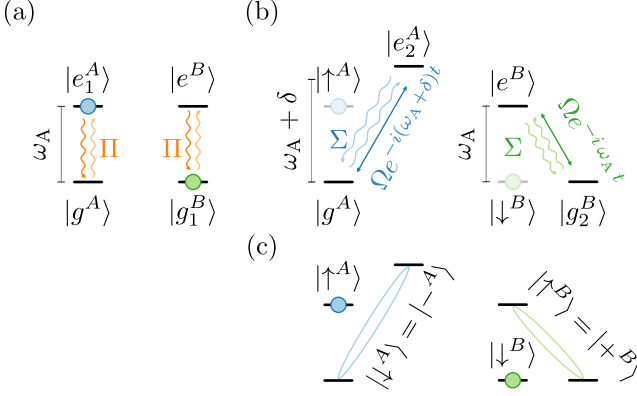


FIG. 11. Level scheme for generating the two-mode squeezing interaction between two atomic ensembles, A and B , mediated by a cavity. (a) Π -polarized light facilitates spin-exchange interactions among all atoms, as described by Eq. (12). The atoms in ensemble A are initially prepared in the $|e_1^A\rangle$ state, while those in ensemble B are initialized in the $|g_1^B\rangle$ state. (b) Resonant driving to auxiliary levels, whose energies are shifted relative to one another, combined with Σ -polarized light, induces effective interactions within each ensemble. This intra-ensemble interaction modifies the global spin-exchange dynamics and gives rise to the desired two-mode squeezing interaction described by Eq. (13). (c) The effective spin-1/2 states of ensemble A are $|\uparrow^A\rangle = |e_1^A\rangle$ and the hybridized state $|\downarrow^A\rangle = |-^A\rangle = \frac{|g_1^A\rangle - |e_2^A\rangle}{\sqrt{2}}$ and $|\downarrow^B\rangle = |g_1^B\rangle$ and $|\uparrow^B\rangle = |-^B\rangle = \frac{|g_2^B\rangle + |e_2^B\rangle}{\sqrt{2}}$.

axis to be perpendicular to the cavity axis, so that the linearly polarized light (Π) and horizontally polarized light (Σ) drive different transitions between the ground and excited-state manifolds. To realize the desired interaction, we isolate three hyperfine states from the ground-state manifold, denoted as $|g^A\rangle, |g_1^B\rangle$, and $|g_2^B\rangle$, along with three states from the excited-state manifold, labeled $|e_1^A\rangle, |e_2^A\rangle$ and $|e^B\rangle$, as illustrated in Fig. 11. The subscripts A and B indicate that atoms in ensemble A exclusively occupy states labeled with A , while atoms in ensemble B are restricted to states labeled with B . The isolation of these energy levels is achieved through appropriate Zeeman and AC Stark shifts. The energy splitting between the isolated ground and excited states is given by ω_A , except for the state $|e_2^A\rangle$, which experiences an additional shift δ relative to $|e_1^A\rangle$ and $|e^B\rangle$.

As sketched in Fig. 11(a), the atoms in ensemble A are prepared in state $|e_1^A\rangle$, while those in ensemble B are initialized in state $|g_1^B\rangle$. The linearly polarized cavity mode drives transitions $|g^A\rangle \leftrightarrow |e_1^A\rangle$ and $|g_1^B\rangle \leftrightarrow |e^B\rangle$. When the cavity is sufficiently far detuned $\Delta = \omega_C - \omega_A \gg g\sqrt{N}$, the cavity mode can be adiabatically eliminated and the unitary evolution of the spins is described by the Hamiltonian in Eq. (12). The underlying process is sketched in Fig. 11(a) where an excited state atom decays to the ground state and emits a linearly polarized photon which can be absorbed by a ground-state atom in the same

or the other ensemble leading to the desired spin-exchange between ensembles but also the undesired spin-exchange between atoms in the same ensemble.

To mitigate the latter effect, we drive the transitions $|g^A\rangle \leftrightarrow |e_2^A\rangle$ and $|g^B\rangle \leftrightarrow |e^B\rangle$ using two lasers with equal Rabi frequency Ω . Additionally, the state $|e_2^A\rangle$ is shifted by an energy δ relative to the other excited states. This additional detuning ensures that vertically polarized photons that drive the same transitions are reabsorbed exclusively by atoms within the same ensemble, thereby inducing effective interactions of the form $J_z^A J_z^A$ and $J_z^B J_z^B$, while suppressing any unwanted inter-ensemble interactions.

To derive this formally we consider the combined system of atoms and the cavity, which is described by an atomic Hamiltonian H_A , light Hamiltonian H_L , and atom-light Hamiltonian H_{AL} . In a rotating frame where $|e_1^A\rangle \rightarrow e^{-i\omega_A t} |e_1^A\rangle$, $|e_2^A\rangle \rightarrow e^{-i(\omega_A + \delta)t} |e_2^A\rangle$, $|e^B\rangle \rightarrow e^{-i\omega_A t} |e^B\rangle$, and $a_P \rightarrow e^{i\omega_A t} a_P$, the Hamiltonians are

$$H_A = \Omega \left(|g^A\rangle \langle e_2^A| + |g_2^B\rangle \langle e^B| + \text{h.c.} \right), \quad (\text{E1})$$

$$H_L = \Delta \sum_{P=\Sigma, \Pi} a_P^\dagger a_P, \quad (\text{E2})$$

and

$$H_{AL} = g \left(e^{i\delta t} a_\Sigma^\dagger c_\Sigma^{e_2^A} |g^A\rangle \langle e_2^A| + a_\Sigma^\dagger c_\Sigma^{e^B} |g_2^B\rangle \langle e^B| + a_\Pi^\dagger c_\Pi^{e_2^A} |g^A\rangle \langle e_1^A| + a_\Pi^\dagger c_\Pi^{e^B} |g_1^B\rangle \langle e^B| + \text{h.c.} \right). \quad (\text{E3})$$

Here $\Delta = \omega_C - \omega_A$, a_P^\dagger is the creation operator of a photon in the respective polarization mode, and c_α^β are the Clebsch-Gordan coefficients between the states $|\alpha\rangle$ and $|\beta\rangle$.

In the following, we consider the dressed-state basis defined by $|\pm^A\rangle = (|e_2^A\rangle \pm |g^A\rangle)/\sqrt{2}$ and $|\pm^B\rangle = (|e^B\rangle \pm |g_2^B\rangle)/\sqrt{2}$. In this basis, the atomic Hamiltonian takes the form

$$H_A = \Omega \left(|+\!^A\rangle \langle +\!^A| - |-\!^A\rangle \langle -\!^A| + |+\!^B\rangle \langle +\!^B| - |-\!^B\rangle \langle -\!^B| \right). \quad (\text{E4})$$

Finally, we express the atom-light interaction Hamiltonian in an interaction picture with respect to H_A and H_L ,

which yields

$$\begin{aligned}
\frac{\sqrt{2}}{g} H_{\text{AL}}^{\text{I}} = & a_{\Pi}^{\dagger} c_{g^A}^{e_1^A} | -^A \rangle \langle e_1^A | e^{-i(\Delta-\Omega)t} + \\
& a_{\Pi}^{\dagger} c_{g_1^B}^{e_1^B} | g_1^B \rangle \langle +^B | e^{-i(\Delta-\Omega)t} + \\
& \frac{a_{\Sigma}^{\dagger} c_{g^A}^{e_2^A} e^{-i(\Delta+\delta)t}}{\sqrt{2}} \left(| +^A \rangle \langle +^A | - \right. \\
& \qquad \qquad \qquad \left. | -^A \rangle \langle -^A | \right) + \\
& \frac{a_{\Sigma}^{\dagger} c_{g_2^B}^{e_2^B} e^{-i\Delta t}}{\sqrt{2}} \left(| +^B \rangle \langle +^B | - \right. \\
& \qquad \qquad \qquad \left. | -^B \rangle \langle -^B | \right) + \\
& + \text{h.c.}, \tag{E5}
\end{aligned}$$

where off-resonant terms that oscillate at frequencies $\Omega + \Delta$, $\Delta - 2\Omega$, and $\Delta + 2\Omega$ are omitted.

Identifying the collective spin operators discussed in the main text as $J_-^A = \sum_i | -^A \rangle_i \langle e^A |$, $J_-^B = \sum_i | g_1^B \rangle \langle +^B |$, $J_z^A = \sum_i \frac{| e^A \rangle_i \langle e^A | - | -^A \rangle_i \langle -^A |}{2}$, and $J_z^B = \sum_i \frac{| +^B \rangle_i \langle +^B | - | g_1^B \rangle_i \langle g_1^B |}{2}$ and adiabatically eliminating the two cavity modes yields an effective many-body spin Hamiltonian of the form

$$\begin{aligned}
H_{\text{eff}} = & \frac{g^2}{2(\Delta-\Omega)} |c_{g^A}^{e_1^A}|^2 (J_-^A + J_-^B) (J_+^A + J_+^B) + \\
& \frac{g^2}{\Delta} |c_{g^A}^{e_2^A}|^2 \left(J_z^A + \frac{N}{4} \right)^2 + \\
& \frac{g^2}{\Delta+\delta} |c_{g_2^B}^{e_2^B}|^2 \left(J_z^B + \frac{N}{4} \right)^2, \tag{E6}
\end{aligned}$$

where we have assumed that $|c_{g^A}^{e_1^A}|^2 = |c_{g_1^B}^{e_1^B}|^2$ and that the number of atoms in both ensembles is exactly the same. The final step is to identify hyperfine states and laser parameters for which $\frac{g^2}{2(\Delta-\Omega)} |c_{g^A}^{e_1^A}|^2 = \frac{g^2}{\Delta} |c_{g^A}^{e_2^A}|^2 = \frac{g^2}{\Delta+\delta} |c_{g_2^B}^{e_2^B}|^2$, such that the effective spin Hamiltonian simplifies to

$$\begin{aligned}
H_{\text{eff}} = & \frac{g^2}{2(\Delta-\Omega)} |c_{g^A}^{e_1^A}|^2 \left(J_-^A J_+^B + J_+^A J_-^B + \mathbf{J}^A \cdot \mathbf{J}^A + \right. \\
& \left. \mathbf{J}^B \cdot \mathbf{J}^B + \frac{N}{2} (J_z^A - J_z^B) \right). \tag{E7}
\end{aligned}$$

By adding an additional field gradient between the two ensembles and assuring that permutation invariance within the subensembles is maintained during the dynamics this yields the Hamiltonian of Eq. (13) up to a $\pi/4$ -rotation under the phase encoding generator.

As a concrete example, we consider the states $|g^A\rangle, |g_1^B\rangle$, and $|g_2^B\rangle$ to correspond to the $9/2, -9/2$, and $-7/2$ levels of the 1S_0 manifold of ^{87}Sr . Similarly, we assign the excited states $|e\rangle_1^A, |e\rangle_2^A$, and $|e^B\rangle$ to the $9/2, 11/2$, and $-9/2$ levels of the 3P_1 manifold, respectively. Furthermore, by choosing $\Delta = (9/8)\Omega$ and $\delta = (1/4)\Omega$, the condition $\frac{g^2}{2(\Delta-\Omega)} |c_{g^A}^{e_1^A}|^2 = \frac{g^2}{\Delta} |c_{g^A}^{e_2^A}|^2 = \frac{g^2}{\Delta+\delta} |c_{g_2^B}^{e_2^B}|^2$ is satisfied.

Appendix F: Analytic expressions for $|J, M\rangle$ states

In this section, we explicitly derive the QFI and other expectation values for the $|J, M\rangle$ states, which exhibit permutational symmetry within the two subensembles. To achieve this, it is convenient to represent the generator of phase encoding in the $|J, M\rangle$ basis as follows:

$$\begin{aligned}
J_z^- = & \sum_{J=1}^{N/2} \sum_{M=-J+1}^J \sqrt{\frac{(J^2-M^2)((N/2+1)^2-J^2)}{4J^2-1}} \\
& \times (|J-1, M\rangle \langle J, M| + \text{h.c.}). \tag{F1}
\end{aligned}$$

In this basis, the generator of phase encoding establishes couplings between states with the same M but J differing by one.

From this expression, it is straightforward to verify that the QFI for the state $|J, M\rangle$ is given by

$$\begin{aligned}
F_{|J, M\rangle}^{\text{Q}} = & 4 \left(\langle J, M | J_z^- J_z^- | J, M \rangle - \langle J, M | J_z^- | J, M \rangle^2 \right) \\
= & \frac{12M^2 + 8J(1+J)(J+J^2-M^2-1)}{3-4J(1+J)} \\
& + \frac{(1-2J(1+J)+2M^2)}{3-4J(1+J)} (N^2+4N). \tag{F2}
\end{aligned}$$

This result simplifies to the expression in Eq. (C2) when J is replaced by $|M|$.

The expectation values of the measurement operator, given by Eq. (6), can be computed in the transformed frame with respect to the phase encoding. This is achieved using identities such as $J_+ J_- = \mathbf{J} \cdot \mathbf{J} - J_z J_z$ and leveraging the fact that the states $|J, M\rangle$ are eigenstates of the operators $\mathbf{J} \cdot \mathbf{J}, J_z, \mathbf{J}^K \cdot \mathbf{J}^K$ for $K = A, B$. The final expression for the measurement expectation value is

$$\begin{aligned}
\langle J, M | \mathcal{M}_\phi | J, M \rangle / \cos(2\phi) (3-4(4J(J+1))) \\
= & J(J+1) (2+M^2-3J(J+1)) \\
& + (J^2+J+M^2-1) (N^2/4+N). \tag{F3}
\end{aligned}$$

Notably, the measurement expectation value for any values of J and M is proportional solely to $\cos(2\phi)$.

For the Lieb-Mattis ground state within a given J_z^+ eigenspace, this expression further simplifies to

$$\begin{aligned}
\langle |M|, M | \mathcal{M}_\phi ||M|, M \rangle / \cos(2\phi) \\
= & \frac{(M+1)(2M-N)(2M+N+4)}{8M+12}. \tag{F4}
\end{aligned}$$

This result highlights that, eigenspaces where $|M| \ll N$, the fringe amplitudes of the measurement operator \mathcal{M} scale quadratically with N . This scaling makes these states particularly promising candidates for robust sensing applications.

Similarly, the expression for $\langle J, M | \mathcal{M}_\phi^2 | J, M \rangle$ can be derived following the same procedure. However, the resulting expression is too extensive to be presented here. Instead, we focus on its dependence on

ϕ , which takes the form $\langle J, M | \mathcal{M}_\phi^2 | J, M \rangle = \alpha(N, J, M) + \beta(N, J, M) \cos(4\phi)$. The general expressions for the real coefficients $\alpha(N, J, M)$ and $\beta(N, J, M)$ simplify to

$$\begin{aligned} \alpha(N, |M|, M) &= \frac{32(3+2M)(5+2M)}{(1+M)(2M-N)(4+2M+N)} \\ &= 4(1+M)(-4+M+M^2) \\ &\quad - 4(2+M)N - (2+M)N^2, \end{aligned} \quad (\text{F5})$$

$$\begin{aligned} \beta(N, |M|, M) &= \frac{32(3+2M)(5+2M)}{(1+M)(2M-N)(4+2M+N)} \\ &= (2+M)(2+2M-N)(6+2M+N), \end{aligned} \quad (\text{F6})$$

for the Lieb-Mattis ground states in different eigenspaces of J_z^\pm .

Substituting the expressions from Eqs. (F4, F5, F6) into the estimator variance defined in Eq. (2), it can be shown that the estimator variance is minimized at $\phi = \pi/4$. Furthermore, under this condition, the estimator variance

saturates the QCRB, which is defined in terms of the QFI given in Eq. (C2).

Appendix G: Average quantum Fisher information

In this section, we discuss a condition under which the convex sum of the QFI of the pure states appearing in the spectral decomposition of a density matrix coincides with the QFI of the density matrix itself. The QFI of a mixed state with spectral decomposition $\rho = \sum_i p_i |\psi_i\rangle \langle \psi_i|$ which is not full rank is given by [85]

$$F_\rho^Q = \sum_i p_i F_{|\psi_i\rangle}^Q - \sum_{i \neq j} \frac{8p_i p_j}{p_i + p_j} |\langle \psi_i | J_z^- | \psi_j \rangle|^2. \quad (\text{G1})$$

For the density matrix in Eq. (15), the states $|\psi_J\rangle = |J, -J\rangle$ which represent the spectral decomposition satisfy $\langle \psi_i | J_z^- | \psi_j \rangle = 0$ for all i, j . Thus the QFI coincides with the average QFI with respect to the probability $p(J)$, see Eq. (17). In general the average QFI is just an upper bound to the actual QFI of a density matrix [86].

-
- [1] G. Rosi, F. Sorrentino, L. Cacciapuoti, M. Prevedelli, and G. Tino, *Nature* **510**, 518 (2014).
 - [2] R. H. Parker, C. Yu, W. Zhong, B. Estey, and H. Müller, *Science* **360**, 191 (2018).
 - [3] C. Overstreet, P. Asenbaum, J. Curti, M. Kim, and M. A. Kasevich, *Science* **375**, 226 (2022).
 - [4] A. Aeppli, K. Kim, W. Warfield, M. S. Safronova, and J. Ye, *Physical Review Letters* **133**, 023401 (2024).
 - [5] T. J. Proctor, P. A. Knott, and J. A. Dunningham, *Physical review letters* **120**, 080501 (2018).
 - [6] W. Ge, K. Jacobs, Z. Eldredge, A. V. Gorshkov, and M. Foss-Feig, *Physical review letters* **121**, 043604 (2018).
 - [7] J. A. Gross and C. M. Caves, *Journal of Physics A: Mathematical and Theoretical* **54**, 014001 (2020).
 - [8] Z. Zhang and Q. Zhuang, *Quantum Science and Technology* **6**, 043001 (2021).
 - [9] J. Bringewatt, I. Boettcher, P. Niroula, P. Bienias, and A. V. Gorshkov, *Physical Review Research* **3**, 033011 (2021).
 - [10] M. Malitesta, A. Smerzi, and L. Pezzè, *Physical Review A* **108**, 032621 (2023).
 - [11] J. B. Fixler, G. Foster, J. McGuirk, and M. Kasevich, *Science* **315**, 74 (2007).
 - [12] D. Durfee, Y. Shaham, and M. Kasevich, *Physical review letters* **97**, 240801 (2006).
 - [13] B. Stray, A. Lamb, A. Kaushik, J. Vovrosh, A. Rodgers, J. Winch, F. Hayati, D. Boddice, A. Stabrawa, A. Niggelbaum, *et al.*, *Nature* **602**, 590 (2022).
 - [14] D. Schlippert, J. Hartwig, H. Albers, L. L. Richardson, C. Schubert, A. Roura, W. P. Schleich, W. Ertmer, and E. M. Rasel, *Physical Review Letters* **112**, 203002 (2014).
 - [15] P. Asenbaum, C. Overstreet, M. Kim, J. Curti, and M. A. Kasevich, *Physical Review Letters* **125**, 191101 (2020).
 - [16] B. Barrett, G. Condon, L. Chichet, L. Antoni-Micollier, R. Arguel, M. Rabault, C. Pelluet, V. Jarlaud, A. Landragin, P. Bouyer, *et al.*, *AVS Quantum Science* **4** (2022).
 - [17] M. Jiang, R. P. Frutos, T. Wu, J. W. Blanchard, X. Peng, and D. Budker, *Physical Review Applied* **11**, 024005 (2019).
 - [18] V. Lucivero, W. Lee, N. Dural, and M. Romalis, *Physical Review Applied* **15**, 014004 (2021).
 - [19] S. Wu, G. Bao, J. Guo, J. Chen, W. Du, M. Shi, P. Yang, L. Chen, and W. Zhang, *Science Advances* **9**, eadg1760 (2023).
 - [20] T. Bothwell, C. J. Kennedy, A. Aeppli, D. Kedar, J. M. Robinson, E. Oelker, A. Staron, and J. Ye, *Nature* **602**, 420 (2022).
 - [21] X. Zheng, J. Dolde, M. C. Cambria, H. M. Lim, and S. Kolkowitz, *Nature Communications* **14**, 4886 (2023).
 - [22] J. M. Robinson, M. Miklos, Y. M. Tso, C. J. Kennedy, T. Bothwell, D. Kedar, J. K. Thompson, and J. Ye, *Nature Physics* **20**, 208 (2024).
 - [23] Y. Yang, M. Miklos, Y. M. Tso, S. Kraus, J. Hur, and J. Ye, *arXiv preprint arXiv:2505.04538* (2025).
 - [24] L. Pezze, A. Smerzi, M. K. Oberthaler, R. Schmied, and P. Treutlein, *Reviews of Modern Physics* **90**, 035005 (2018).
 - [25] J. Huang, M. Zhuang, and C. Lee, *Applied Physics Reviews* **11** (2024).
 - [26] G. Foster, J. Fixler, J. McGuirk, and M. Kasevich, *Optics letters* **27**, 951 (2002).
 - [27] G. Rosi, L. Cacciapuoti, F. Sorrentino, M. Menchetti, M. Prevedelli, and G. Tino, *Physical Review Letters* **114**, 013001 (2015).
 - [28] B. Barrett, L. Antoni-Micollier, L. Chichet, B. Battenier, T. Léveque, A. Landragin, and P. Bouyer, *Nature communications* **7**, 13786 (2016).
 - [29] M. Langlois, R. Caldani, A. Trimeche, S. Merlet, and F. Pereira dos Santos, *Physical Review A* **96**, 053624 (2017).

- [30] G. E. Marti, R. B. Hutson, A. Goban, S. L. Campbell, N. Poli, and J. Ye, *Physical review letters* **120**, 103201 (2018).
- [31] E. R. Elliott, D. C. Aveline, N. P. Bigelow, P. Boegel, S. Botsi, E. Charron, J. P. d’Incao, P. Engels, T. Estrampes, N. Gaaloul, *et al.*, *Nature* **623**, 502 (2023).
- [32] D. J. Wineland, J. J. Bollinger, W. M. Itano, F. Moore, and D. J. Heinzen, *Physical Review A* **46**, R6797 (1992).
- [33] M. Kitagawa and M. Ueda, *Physical Review A* **47**, 5138 (1993).
- [34] J. Ma, X. Wang, C.-P. Sun, and F. Nori, *Physics Reports* **509**, 89 (2011).
- [35] W. J. Eckner, N. Darkwah Oppong, A. Cao, A. W. Young, W. R. Milner, J. M. Robinson, J. Ye, and A. M. Kaufman, *Nature* **621**, 734 (2023).
- [36] R. Corgier, M. Malitesta, L. A. Sidorenkov, F. P. D. Santos, G. Rosi, G. M. Tino, A. Smerzi, L. Salvi, and L. Pezzè, *arXiv preprint arXiv:2501.18256* (2025).
- [37] S. Altenburg, M. Oszmaniec, S. Wölk, and O. Gühne, *Physical Review A* **96**, 042319 (2017).
- [38] Z. Eldredge, M. Foss-Feig, J. A. Gross, S. L. Rolston, and A. V. Gorshkov, *Physical Review A* **97**, 042337 (2018).
- [39] P. Sekatski, S. Wölk, and W. Dür, *Physical Review Research* **2**, 023052 (2020).
- [40] A. Hamann, P. Sekatski, and W. Dür, *Quantum Science and Technology* **7**, 025003 (2022).
- [41] A. Hamann, P. Sekatski, and W. Dür, *Quantum Science and Technology* **9**, 035005 (2024).
- [42] J. Bate, A. Hamann, M. Canteri, A. Winkler, Z. X. Koong, V. Krutyanskiy, W. Dür, and B. P. Lanyon, *arXiv preprint arXiv:2501.08940* (2025).
- [43] J. J. Bollinger, W. M. Itano, D. J. Wineland, and D. J. Heinzen, *Physical Review A* **54**, R4649 (1996).
- [44] A. Periwal, E. S. Cooper, P. Kunkel, J. F. Wienand, E. J. Davis, and M. Schleier-Smith, *Nature* **600**, 630 (2021).
- [45] S. L. Braunstein and C. M. Caves, *Physical Review Letters* **72**, 3439 (1994).
- [46] M. G. Paris, *International Journal of Quantum Information* **7**, 125 (2009).
- [47] R. Demkowicz-Dobrzański, M. Jarzyna, and J. Kołodyński, *Progress in Optics* **60**, 345 (2015).
- [48] A. Omran, H. Levine, A. Keesling, G. Semeghini, T. T. Wang, S. Ebadi, H. Bernien, A. S. Zibrov, H. Pichler, S. Choi, *et al.*, *Science* **365**, 570 (2019).
- [49] I. Pogorelov, T. Feldker, C. D. Marciniak, L. Postler, G. Jacob, O. Kriegelsteiner, V. Podlesnic, M. Meth, V. Negnevitsky, M. Stadler, *et al.*, *PRX quantum* **2**, 020343 (2021).
- [50] G. J. Mooney, G. A. White, C. D. Hill, and L. C. Hollenberg, *Journal of Physics Communications* **5**, 095004 (2021).
- [51] S. A. Moses, C. H. Baldwin, M. S. Allman, R. Ancona, L. Ascarrunz, C. Barnes, J. Bartolotta, B. Bjork, P. Blanchard, M. Bohn, *et al.*, *Physical Review X* **13**, 041052 (2023).
- [52] H. Cable and G. A. Durkin, *Physical review letters* **105**, 013603 (2010).
- [53] B. Sundar, D. Barberena, A. P. Orioli, A. Chu, J. K. Thompson, A. M. Rey, and R. J. Lewis-Swan, *Physical Review Letters* **130**, 113202 (2023).
- [54] M. Mamaev, M. Koppenhöfer, A. Pocklington, and A. A. Clerk, *Physical review letters* **134**, 073603 (2025).
- [55] I. Urizar-Lanz, P. Hyllus, I. L. Egusquiza, M. W. Mitchell, and G. Tóth, *Physical Review A—Atomic, Molecular, and Optical Physics* **88**, 013626 (2013).
- [56] G. Vidal and R. Tarrach, *Physical Review A* **59**, 141 (1999).
- [57] W. Dür, G. Vidal, and J. I. Cirac, *Physical Review A* **62**, 062314 (2000).
- [58] X. Wang and K. Mølmer, *The European Physical Journal D—Atomic, Molecular, Optical and Plasma Physics* **18**, 385 (2002).
- [59] A. Neven, J. Martin, and T. Bastin, *Physical Review A* **98**, 062335 (2018).
- [60] C.-J. Lin, Z.-W. Liu, V. V. Albert, and A. V. Gorshkov, *arXiv preprint arXiv:2409.20561* (2024).
- [61] J. A. Muniz, D. Barberena, R. J. Lewis-Swan, D. J. Young, J. R. Cline, A. M. Rey, and J. K. Thompson, *Nature* **580**, 602 (2020).
- [62] Z. Kurucz and K. Mølmer, *Physical Review A—Atomic, Molecular, and Optical Physics* **81**, 032314 (2010).
- [63] B. A. Chase and J. Geremia, *Physical Review A—Atomic, Molecular, and Optical Physics* **78**, 052101 (2008).
- [64] Z.-X. Gong, M. Xu, M. Foss-Feig, J. K. Thompson, A. M. Rey, M. Holland, and A. V. Gorshkov, *arXiv preprint arXiv:1611.00797* (2016).
- [65] N. Shammah, S. Ahmed, N. Lambert, S. De Liberato, and F. Nori, *Physical Review A* **98**, 063815 (2018).
- [66] T. Nadolny, C. Bruder, and M. Brunelli, *Physical Review X* **15**, 011010 (2025).
- [67] Y. Zhang, Y.-X. Zhang, and K. Mølmer, *New Journal of Physics* **20**, 112001 (2018).
- [68] S. J. Masson and S. Parkins, *Physical Review Letters* **122**, 103601 (2019).
- [69] M. A. Norcia, R. J. Lewis-Swan, J. R. Cline, B. Zhu, A. M. Rey, and J. K. Thompson, *Science* **361**, 259 (2018).
- [70] W. R. Milner, S. Lannig, M. Mamaev, L. Yan, A. Chu, B. Lewis, M. N. Frankel, R. B. Hutson, A. M. Rey, and J. Ye, *arXiv preprint arXiv:2402.13398* (2024).
- [71] J. Franke, S. R. Muleady, R. Kaubruegger, F. Kranzl, R. Blatt, A. M. Rey, M. K. Joshi, and C. F. Roos, *Nature* **621**, 740 (2023).
- [72] G. Bornet, G. Emperauger, C. Chen, B. Ye, M. Block, M. Bintz, J. A. Boyd, D. Barredo, T. Comparin, F. Mez-zacapo, *et al.*, *Nature* **621**, 728 (2023).
- [73] J. A. Hines, S. V. Rajagopal, G. L. Moreau, M. D. Wahrman, N. A. Lewis, O. Marković, and M. Schleier-Smith, *Physical Review Letters* **131**, 063401 (2023).
- [74] R. Kaubruegger, P. Silvi, C. Kokail, R. van Bijnen, A. M. Rey, J. Ye, A. M. Kaufman, and P. Zoller, *Physical review letters* **123**, 260505 (2019).
- [75] B. Koczor, S. Endo, T. Jones, Y. Matsuzaki, and S. C. Benjamin, *New Journal of Physics* **22**, 083038 (2020).
- [76] R. Kaubruegger, D. V. Vasilyev, M. Schulte, K. Hammerer, and P. Zoller, *Physical review X* **11**, 041045 (2021).
- [77] J. Yu, S. R. Muleady, Y.-X. Wang, N. Schine, A. V. Gorshkov, and A. M. Childs, *arXiv preprint arXiv:2411.03428* (2024).
- [78] A. Piñeiro Orioli and A. M. Rey, *Physical Review Letters* **123**, 223601 (2019).
- [79] S. Gammelmark and K. Mølmer, *Physical review letters* **112**, 170401 (2014).
- [80] A. Shankar, G. P. Greve, B. Wu, J. K. Thompson, and M. Holland, *Physical Review Letters* **122**, 233602 (2019).
- [81] D. Yang, S. F. Huelga, and M. B. Plenio, *Physical Review X* **13**, 031012 (2023).
- [82] J. Duan, Z. Hu, X. Lu, L. Xiao, S. Jia, K. Mølmer, and Y. Xiao, *Nature Physics* , 1 (2025).

- [83] A. Beekman, L. Rademaker, and J. Van Wezel, *SciPost Physics Lecture Notes* , 011 (2019).
- [84] L. Rademaker, *Physical Review Research* **1**, 032018 (2019).
- [85] J. Liu, X.-X. Jing, W. Zhong, and X.-G. Wang, *Communications in Theoretical Physics* **61**, 45 (2014).
- [86] L. Pezze and A. Smerzi, in *Atom interferometry* (IOS Press, 2014) pp. 691–741.